Activation of Notch Signaling in a Xenograft Model of Brain Metastasis

Do-Hyun Nam,[1] Hye-Min Jeon,[3] Shiyeon Kim,[1] Mi Hyun Kim,[1] Young-Ju Lee,[4] Min Su Lee,[6] Hyunggee Kim,[3] Kyeung Min Joo,[1] Dong-Sup Lee,[5] Janet E. Price,[7] Sa Ik Bang,[2] and Woong-Yang Park[4]

Abstract

Purpose: The potential of metastasis can be predicted from clinical features like tumor size, histologic grade, and gene expression patterns. We examined the whole-genome transcriptomic profile of a xenograft model of breast cancer to understand the characteristics of brain metastasis.

Experimental Design: Variants of the MDA-MB-435 cell were established from experimental brain metastases. The LvBr2 variant was isolated from lesions in a mouse injected in the left ventricle of the heart, and these cells were used for two cycles of injection into the internal carotid artery and selection of brain lesions, resulting in the Br4 variant. To characterize the different metastatic variants, we examined the gene expression profile of MDA-MB-435, LvBr2, and Br4 cells using microarrays.

Results: We could identify 2,016 differentially expressed genes in Br4 by using the F test. Various metastasis-related genes and a number of genes related to angiogenesis, migration, tumorigenesis, and cell cycle were differentially expressed by the Br4 cells. Notably, the Notch signaling pathway was activated in Br4, with increased *Jag2* mRNA, activated Notch intracellular domain, and Notch intracellular domain/CLS promoter-luciferase activity. Br4 cells were more migratory and invasive than MDA-MB-435 cells in collagen and Matrigel Transwell assays, and the migration and invasion of Br4 cells were significantly inhibited by inactivation of Notch signaling using DAPT, a γ-secretase inhibitor, and RNA interference–mediated knockdown of Jagged 2 and Notch1.

Conclusions: Taken together, these results suggest that we have isolated variants of a human cancer cell line with enhanced brain metastatic properties, and the activation of Notch signaling might play a crucial role in brain metastasis.

Monitoring tumor metastasis in patients can be critical for deciding the strategy for treatment and prognosis of patients. During the process of metastasis, tumor cells must survive and overcome physical barriers and must be able to grow in the new tissue environments. How cancer cells acquire metastatic abilities has been a long-standing question (1). Molecular profiling of tumors provides a better system for classifying cancers, a clarification of the origin of these diseases, a more accurate prognostic capacity than was previously available, and an improved ability to choose among possible therapies. Progress in molecular profiling of solid tumors began with the identification of sets of genes whose expression could be used to classify breast cancers (2) and to predict clinical outcome (3, 4).

Dormant human cancer cells isolated from metastasis-free organs of animals carrying primary tumors can reactivate their tumorigenic and metastatic potency (5). This is one of the characteristics of cancer stem cells. Cancer stem cells are

Authors' Affiliations: [1]Neurosurgery and [2]Plastic and Reconstructive Surgery, Samsung Medical Center and Samsung Biomedical Research Institute, Sungkyunkwan University School of Medicine, [3]Cell Growth Regulation Laboratory, Division of Biotechnology, College of Life Sciences and Biotechnology, Korea University, [4]Genomic Medicine Institute, MRC and Department of Biochemistry and Molecular Biology, [5]Cancer Research Institute, College of Medicine, [6]Biointelligence Laboratory, School of Computer Science and Engineering, Seoul National University, Seoul, Republic of Korea, and [7]Department of Cancer Biology, The University of Texas M. D. Anderson Cancer Center, Houston, Texas

Received 8/29/07; revised 3/4/08; accepted 3/25/08.

Grant support: SRC program of KOSEF (Research Center for Women's Diseases) and a Korea Science and Engineering Foundation (KOSEF) grant funded by the Korean Government (MOST; no. MM10641000104-06N4100-1040; D-H. Nam, M20706000020-07M0600-02010; W-Y. Park), and the National R&D Program for Cancer Control, Ministry of Health and Welfare (0720030; H. Kim).

The costs of publication of this article were defrayed in part by the payment of page charges. This article must therefore be hereby marked *advertisement* in accordance with 18 U.S.C. Section 1734 solely to indicate this fact.

Note: Supplementary data for this article are available at Clinical Cancer Research Online (http://clincancerres.aacrjournals.org/).

D-H. Nam and H-M. Jeon contributed equally to this work.

S.I. Bang and W-Y. Park share senior authorship.

Requests for reprints: Woong-Yang Park, Genomic Medicine Institute, MRC and Department of Biochemistry and Molecular Biology, College of Medicine, Seoul National University, 28 Yongondong, Chongnogu, Seoul 110-799, Republic of Korea. Phone: 82-2-740-8241; Fax: 82-2-744-4534; E-mail: wypark@snu.ac.kr or Sa Ik Bang, Department of Plastic and Reconstructive Surgery, Samsung Medical Center and Samsung Biomedical Research Institute, Sungkyunkwan University School of Medicine, 50 Ilwon-Dong, Kangnam-Ku, Seoul, 135-710, Republic of Korea. Phone: 82-2-3410-2215; Fax: 82-2-3410-0036; E-mail: sibang55@skku.edu.

doi:10.1158/1078-0432.CCR-07-4039

thought to be maintained, and to retain their proliferating capacity, through the influence of a stem cell niche. The niches can influence differentiated cells to be transformed into tumors by inducing dedifferentiation. The Notch signaling pathway may be important for communication between stem cells and niche cells (6).

The classical role of Notch receptors (Notch 1-4) is signaling to determine cell fates through interaction with their ligands (Jagged 1-2, and Delta-like 1-4 in mammals; ref. 7). The interaction between Notch receptors and their ligands causes two-step proteolysis of the receptors. This results in an active form of the Notch intracellular domain (NICD) that translocates from the cytoplasm to the nucleus, and ultimately acts as a transcriptional activator, stimulating the expression of various genes, such as Hes1 and Hey1, which are associated with the inhibition of neuronal differentiation (8).

The MDA-MB-435 human cancer cell line can form brain metastases when injected into the internal carotid artery (ICA) or the left ventricle of the heart of immunodeficient mice (9). In the present study, we have established brain metastatic cells (Br4 cells) from MDA-MB-435 cells, and characterized molecular and cellular mechanisms governing brain metastasis using Br4 cells.

Materials and Methods

Cell culture conditions, cell cycle, and apoptosis analysis. MDA-MB-435 cells, LvBr2, and Br4 cells were maintained in Eagle's minimal essential medium enriched with 10% fetal bovine serum (Hyclone), 1% penicillin and streptomycin (Life Technologies), and 2 mmol/L of L-glutamine (Life Technologies). The DNA content of trypsinized cells was determined by staining with propidium iodide using a Cellular DNA Flow Cytometric Analysis kit (Roche). Cell cycle analysis was carried out by FACSCalibur (BD Bioscience) and analyzed using a CellQuest software program (BD Bioscience). The apoptotic death rates of cells treated with or without *N*-[N-(3,5-Difluorophenacetyl-L-alanyl)]-*S*-phenylglycine t-butyl DAPT (10 μmol/L) for 3 days were determined by Annexin V/propidium iodide staining.

Mouse inoculation. To produce brain metastases, mice were anesthetized with Nembutal sodium, restrained on a corkboard, and placed under a dissecting microscope as described previously (5). The ICA was prepared for an injection. A ligature of 4-0 silk suture was placed on the distal part of the common carotid artery and a second ligature was placed and loosely tied around the proximal part of the ICA. A sterile cotton tip applicator was inserted under the artery just distal to the injection site to elevate the ICA. This procedure controlled bleeding from the carotid artery by back-flow from distal vessels. The proximal ICA between the two ligatures was nicked with a pair of microscissors, and a <30-gauge polyethylene cannula was inserted into the lumen. To assure proper delivery, the cells (5×10^4 MDA-MB-435, LvBr2, or Br3/100 μL HBSS) were injected slowly. The second ligature was then tightened, and the skin closed with sutures (5).

Microarray and data analysis. Total RNAs from MDA-MB-435 and its derivative cells were isolated using TRIzol (Invitrogen) and the RNeasy mini kit (Qiagen) as described previously (10). The purity and integrity of the total RNA were checked by Bioanalyzer (Agilent). Probe synthesis from total RNA samples, hybridization, detection, and scanning were done according to standard protocols from Affymetrix, Inc. For data analysis, fluorescence intensity was processed and measured using a GeneChip scanner 3000. By applying robust multiarray averaging as a normalization process, the raw intensity values are background-corrected, $\log_2$-transformed, and then quantile-normalized. The multivariate permutation test was used to provide 95% confidence that the false discovery rate was <1%. The false discovery rate is the proportion of the list of genes claimed to be differentially expressed to be false positives (11).

Reverse transcription-PCR. A portion (1 μL) of the reverse transcription reaction was used to amplify Hes1, Hey1, Jagged2, Notch1, and GAPDH fragments using human-specific primer sets. Information on primer sequences and PCR variables can be provided upon request. All reverse transcription-PCR (RT-PCR) amplifications were verified to be within the linear range.

Luciferase-reporter activity assay. The relative luciferase activities of NICD/CLS transcriptional activity in the MDA-MB-435 cells and Br4 cells were determined by transfection of pGL3-basic plasmid (as a negative control), pGL3-CLS plasmid and pGL3-Wnt3a plasmid (as a nonspecific control) using the Dual-Glo Luciferase Assay System (Promega). Transfection efficiency was normalized with the activity of Renilla luciferase, which was cotransfected with the aforementioned pGL3-luciferase-reporter constructs.

Western blot analysis. Whole cell extracts were prepared using radioimmunoprecipitation assay lysis buffer containing protease inhibitor (Roche). Protein in the extracts (50 μg) was separated by a 4% to 12% gradient SDS-PAGE NuPAGE gel (Invitrogen) and transferred to polyvinylidene difluoride membrane (Millipore). The membranes were blocked with 5% nonfat milk and incubated with anti-cleaved Notch1 (Val1774; Cell Signaling Technology) and anti–α-tubulin (Sigma) antibodies. Membranes were then incubated with horseradish peroxidase–conjugated anti–secondary IgG (Pierce) antibody and visualized with SuperSignal West Pico Chemiluminescent Substrate (Pierce).

In vitro *cell migration and invasion assays.* *In vitro* migration of MDA-MB-435 cells and Br4 cells through transwell filters was monitored to check the metastatic potential of each cell. Briefly, cells (4×10^4) were seeded on the upper chamber of transwells (8 μm pore diameter; BD Bioscience) that were coated on the underside without or with 0.01% collagen I (BD Bioscience) or 50% Matrigel (BD Bioscience). Then, cells were allowed to grow in medium (Eagle's minimal essential medium + 10% fetal bovine serum) in both upper and lower chambers for 12, 37, and 72 h. Cells (4×10^4) were also allowed to grow in the uncoated upper chamber of transwells in the different concentrations of DAPT (0, 3, 5, and 10 μmol/L; Calbiochem) for 3 days. After incubation for the aforementioned times, cells were photographed and cell numbers were counted using a hemacytometer.

Construction of RNA interference expression vector and transduction. Cells were infected with PT67 packaging cell–derived retrovirus, which harbors pSuperRetro-Notch1-RNAi-Puro and pSuperRetro-Jagged2-RNAi-Puro expression vectors (Oligoengine). The target sequences were human Notch1-RNAi, aaagatatgcagaacaacagg; and human Jagged2-RNAi, aagttcctctcacacaaattc.

Immunofluorescence. Cells fixed with 4% paraformaldehyde were incubated with primary anti-cleaved Notch1 (Val1744; Cell Signaling Technology), anti-Hey1 (AB5714; Chemicon), and anti-Hes1 (AB5702; Chemicon) antibodies for 12 h at 4°C. Nuclei were then stained with 4′,6-diamidino-2-phenylindole (1 μg/mL) for 5 min. Fluorescence images were obtained using a confocal laser scanning microscope (LSM5 Pascal; Carl Zeiss).

Results

Modeling of brain metastasis using MDA-MB-435 human cancer cells. LvBr2 cells were isolated from metastatic brain lesions in a nude mouse injected with MDA-MB-435 cells in the left ventricle of the heart (9). To increase the metastatic potential of LvBr2 into the brain, we injected MDA-MB-435 LvBr2 cells into the ICA of BALB/c nude mice and cultured Br3 from LvBr2 brain tumors, and then repeated the procedure to produce the Br4 subclone. At each step, H2Kd+ mouse cells were excluded from the recovered cultures (<2%) by fluorescence-activated cell sorting to ensure that the Br3 and Br4 subclones were of human origin.

We tested the biological features and metastatic characteristics of MDA-MB-435, LvBr2, and Br4 cells by injecting 5×10^4 cells into the ICA or mammary fat pad of nonobese diabetic/severe combined immunodeficiency or BALB/c nude mouse. When cells were injected in the ICA, the resulting brain lesions of each cell line showed similar histologic features (Fig. 1A), but the survival of Br4-injected mice was significantly shorter than that of mice injected with the original cell line (Fig. 1B). When cells were injected into the mammary fat pad, MDA-MB-435 and LvBr2 cells produced local tumors as previously reported (9). However, Br4 did not make visible tumors in the injection site (Fig. 1C), yet they did form metastatic tumor nodules in the lungs of some mice (Fig. 1D). These results suggested that Br4 cells carry the characteristics of human cancer cells that tend to metastasize rather than form large tumors at the primary site. Furthermore, the Br4 cells grow more aggressively in the brain than MDA-MB-435 and LvBr2 cells.

Cell morphology, in vitro growth kinetics, migration, and invasion of Br4 cells. In the early passages of cell culture, most Br4 cells displayed a relatively round and brilliant morphology, and were weakly attached to the substrate of the culture dish compared with the parental MDA-MB-435 cells when grown in Eagle's minimal essential medium + 10% fetal bovine serum (Fig. 2A). However, during continuous passages (almost after 20 passages), a unique Br4 cell morphology was shown to revert to that of the MDA-MB-435 cells, with relatively flattened and spindle-shaped cells that were more firmly attached to the substrate (data not shown). Therefore, to determine the cell growth kinetics, migration, and invasion characteristics of Br4 cells *in vitro*, we used relatively early passage cells (passage 13), at which most of these cells was still round and brilliant. Br4 cells were found to grow relatively faster (Fig. 2B), and in addition, have significantly fewer cells in G_1, and more in S phase than MDA-MB-435 cells, measured by fluorescence-activated cell sorting analysis (Fig. 2C).

Profiling the characteristics of metastatic brain cancer cells. The gene expression profiles of three cell lines, MDA-MB-435, LvBr2, and Br4, were analyzed using Affymetrix

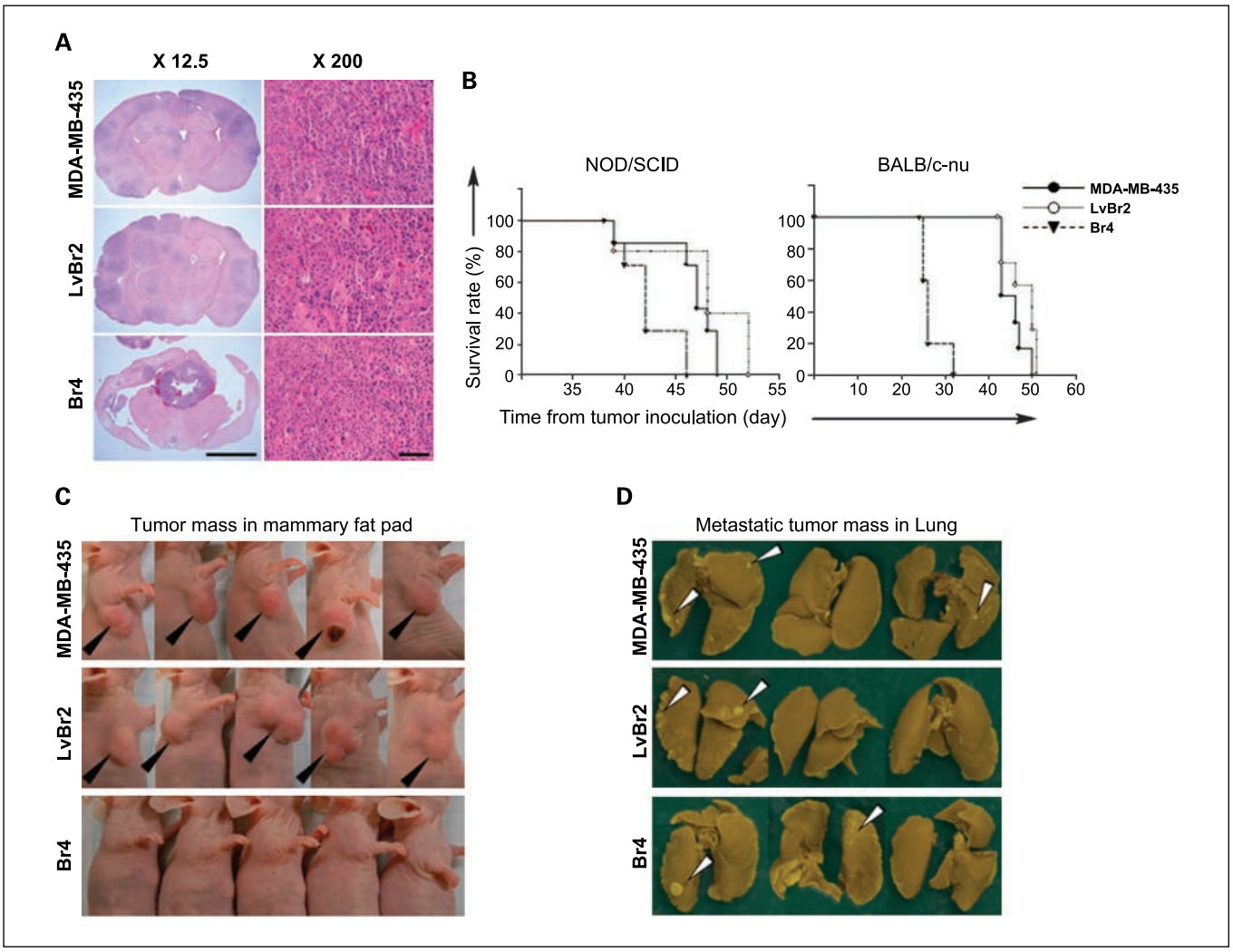

Fig. 1. Tumorigenesis and survival of MDA-MB-435 cells. *A,* tumor tissues from brain metastasis of MDA-MB-435 and Br4 cells in immunodeficient mice revealed no differences according to pathologic analysis (*bar,* 100 μm). *B,* survival rate of animals injected with MDA-MB-435, LvBr2, and Br4 cells were analyzed in two experiments using either nonobese diabetic/severe combined immunodeficiency (NOD/SCID; $n = 19$) or BALB/c nude mice (BALB/c-nu; $n = 18$). Tumor formation in the mammary fat pads (*C*) and the patterns of lung metastasis (*D*) revealed the unique tumorigenic and metastatic phenotype of the Br4 variant cell line.

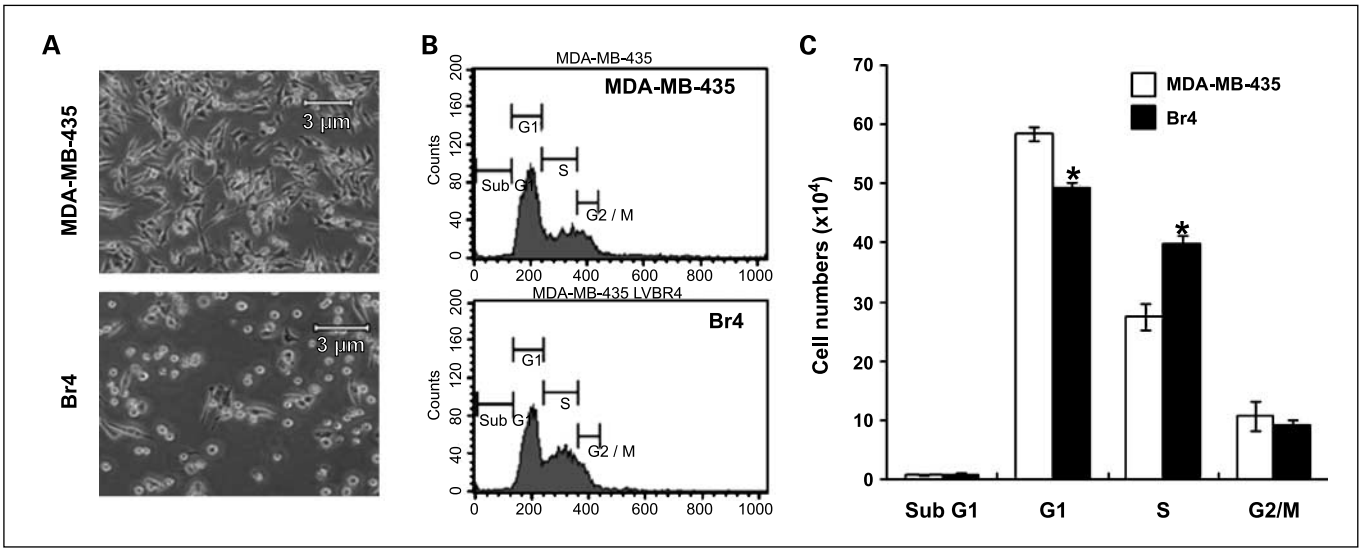

Fig. 2. Cell morphology and growth kinetics of the MDA-MB-435 and Br4 cells. *A,* representative photos of MDA-MB-435 cells and Br4 cells (magnification, ×40). *B,* representative cell cycle profile of MDA-MB-435 (*top*) and Br4 cells (*bottom*) that was determined by fluorescence-activated cell sorting analysis. *C,* quantitative analysis of cell cycle profile of MDA-MB-435 and Br4 cells. *, $P < 0.05$, statistical difference ($n = 3$).

Human Genome U133 Plus 2.0 arrays containing more than 47,000 human transcripts. After normalization of data from biologically triplicated samples, we selected 4,378 differentially expressed genes in one of three groups (false discovery rate, 95%; $P < 0.001$). We plotted the chromosomal location of the differentially expressed genes using ChromoViz (12), but did not identify clustering of differentially expressed genes on any human chromosome (Supplementary Fig. S1), which suggested that the altered expression patterns did not involve chromatin regulation. Next, we focused on genes differentially expressed in Br4 in order to understand the characteristics of cancer cells metastatic to the brain. Among the 4,378 differentially expressed genes, 1,182 genes were significantly up-regulated and 834 genes were down-regulated ($P < 0.001$) in Br4 cells compared with the original MDA-MB-435 cells. When grouped by Gene Ontology categories, genes related to chemotaxis and locomotion, RNA processing, and growth signaling were up-regulated, whereas classes of genes related to energy metabolism, cell adhesion, and cell cycle arrest were significantly down-regulated (Supplementary Table S1). Up-regulation and down-regulation of multiple transcripts might work together to produce the enhanced metastatic phenotype of the Br4 cells.

From the list of 2,016 differentially expressed genes, functionally annotated genes were selected and classified into several clusters that might explain the phenotype of Br4 cells. In Table 1, we summarize the genes and classes relative to their possible functions. Possibly related to the high potential of Br4 cells to metastasize to the brain, the expressions of proangiogenic genes ANGPT1, ANGPT2, and VEGF were increased, whereas the expressions of THBS1 and THBS2 were decreased. In addition, many oncogenes, growth factors, and antiapoptotic genes were up-regulated, whereas cell cycle inhibitors and proapoptotic genes were down-regulated.

More interestingly, we identified eight genes related to Notch signaling in the list of genes differentially expressed in Br4 cells. To validate the changes in their mRNA levels, four genes were selected for analysis by real-time RT-PCR (Fig. 3A). Among them, JAG2, a ligand for Notch was up-regulated in Br4 cells, which might suggest the activation of Notch signaling pathways in Br4 cells.

Notch signaling in Br4 metastatic cancer cells. Because JAG2 was shown to be up-regulated in Br4 cells compared with MDA-MB-435 cells, we further compared the expression levels of the activated form of Notch 1 (NICD) by Western blot analysis using an NICD-specific antibody (that recognizes an active Notch cleaved at valine 1771 of Notch1). As determined by Western blot and semiquantitative RT-PCR, expression of active Notch1 protein (Fig. 3B, *top left*) and its downstream genes, such as Hey1 and Hes1 mRNAs (Fig. 3B, *bottom left graph*), was relatively increased in Br4 cells compared with MDA-MB-435 cells. Furthermore, we found that increased Hey1 and Hes1 proteins in Br4 cells were mainly located in the nucleus (Fig. 3B, *right photos*). In agreement with this result, as determined by CLS promoter-luciferase assay, NICD/CLS transcriptional activity was significantly elevated in the Br4 cells compared with MDA-MB-435 cells (Fig. 3C, *top graph*). A majority of active Notch1 were found to be localized in the nucleus of Br4 cells as determined by immunofluorescence analysis (Fig. 3C, *bottom photos*). Taken together, these results suggest that transcriptional activation of JAG2, one of the Notch ligands, might be sufficient to activate Notch receptor and ultimately stimulate Notch signaling in Br4 cells.

Migration and invasion of Br4 cells regulated by Notch. Because Br4 cells were initially established from brain metastases in a nude mouse injected with cells into the ICA, we reasoned that Br4 cells should be more migratory and invasive than the original MDA-MB-435 cells. To test this, we conducted *in vitro* migration and invasion assays using a transwell culture system in which cells were plated onto membranes that were either uncoated, or coated with collagen or Matrigel (Supplementary Fig. S2). As shown in

Fig. 4A, significantly more Br4 cells migrated through both uncoated and collagen-coated membranes of transwell chambers, compared with MDA-MB-435 cells. Almost no migration was scored for MCF7 cells, which were used as a negative control of the cell migration assay. Furthermore, when compared with MDA-MB-435 cells, more Br4 cells invaded into Matrigel-coated membranes (Fig. 4B). These results suggest that the brain metastasis–selected Br4 cells, with enhanced migration and invasive properties, may represent a selected subpopulation of the heterogeneous MDA-MB-435 cell line.

Next, we determined whether the activated Notch signaling pathway contributes to the increased migration of Br4 cells using the transwell culture system and DAPT, a specific inhibitor of γ-secretase. We found that the expression levels of active Notch1 protein were markedly decreased in DAPT-treated Br4 cells compared with control Br4 cells (Fig. 4C). In agreement with this result, expression of Hey1 and Hes1 protein was also dramatically decreased in the Br4 cells by DAPT treatment (Fig. 4D). The migration of Br4 cells was significantly decreased in the presence of 5 and 10 μmol/L of DAPT. The migration of the MDA-MB-435 cells was almost unchanged in the presence of 5 μmol/L of DAPT, whereas there was a significant decrease at the higher concentration of 10 μmol/L of DAPT (Fig. 4E; Supplementary Fig. S3). We also confirmed that the decreased migration of Br4 cells by DAPT-mediated inhibition of Notch signaling is not caused by either a decreased cell growth rate or increased apoptosis by DAPT treatment because the apoptotic rate of the Br4 cells was not changed by DAPT treatment and the cell growth rate of the Br4 cells was even slightly increased following treatment with DAPT (Supplementary Fig. S4). To further validate the role of Notch signaling in the migration and invasion of Br4 cells, we depleted Jagged2 and Notch1 expression in Br4 cells using Jagged2-specific and Notch1-specific RNA interference (RNAi) expression vectors. We found that the expression levels of Jagged2 and Notch1 mRNAs in the Br4-Jag2-RNAi and Br4-Notch1-RNAi cells, respectively, were significantly decreased as compared with those in their counterpart control cells (Fig. 5A). Similar to their expression levels, the Br4 cells transduced with Jag2-RNAi or Notch1-RNAi expression vectors showed robust decreases of migration and invasion under

Table 1. Selected list of differentially expressed genes in Br4 cells

Function	Symbol	Gene name	GenBank no.
Up-regulated genes			
Angiogenesis	*ANGPT1*	Angiopoietin 1	NM_001146
	ANGPT2	Angiopoietin 2	NM_001147
	VEGF	Vascular endothelial growth factor	M27281
Oncogene	*FES*	Feline sarcoma oncogene	NM_002005
	JUN	v-jun sarcoma virus 17 oncogene homologue (avian)	BC002646
	MERTK	c-mer proto-oncogene tyrosine kinase	NM_006343
	NRAS	Neuroblastoma RAS viral (v-ras) oncogene homologue	NM_002524
	RRAS2	Related RAS viral (r-ras) oncogene homologue 2	AI431643
	SRC	v-Src sarcoma viral oncogene homologue (avian)	AK024281
Growth factor	*EGFR*	Epidermal growth factor receptor	NM_005228
	FGF1	Fibroblast growth factor 1 (acidic)	NM_033136
	FGFR1	Fibroblast growth factor receptor 1	M63889
Cell cycle	*CDC25C*	Cell division cycle 25C	NM_001790
	CDC27	Cell division cycle 27	NM_001256
	CDCA4	Cell division cycle associated 4	NM_017955
	GADD45A	Growth arrest and DNA damage–inducible, α	NM_001924
Stem cell	*MSI2*	Musashi homologue 2 (Drosophila)	BC001526
	WNT3	Wingless-type MMTV integration site family, member 3	AA463626
Apoptosis	*BCL10*	B cell CLL/lymphoma 10	AF082283
	BCL2L1	BCL2-like 1	NM_001191
	BIRC4	Baculoviral IAP repeat-containing 4	N30645
	FAIM	Fas apoptotic inhibitory molecule	NM_018147
Notch signaling	*HDAC3*	Histone deacetylase 3	AF059650
	JAG2	Jagged 2	AF029778
	NUMB	Numb homologue (Drosophila)	NM_003744
	APH1B	Anterior pharynx defective 1 homologue B (*C. elegans*)	NM_031301
	HES4	Hairy and enhancer of split 4 (Drosophila)	NM_021170
	PSEN1	Presenilin 1 (Alzheimer disease 3)	NM_007318
miRNA	*EIF2C2*	Eukaryotic translation initiation factor 2C, 2	BF223464
	MIRN21	MicroRNA 21	BF674052
Down-regulated genes			
Angiogenesis	*THBS1*	Thrombospondin 1	NM_003246
	THBS2	Thrombospondin 2	NM_003247
Cell cycle	*CDKN2A*	Cyclin-dependent kinase inhibitor 2A (p16)	NM_000077
Notch signaling	*DNER*	Δ-notch–like EGF repeat–containing transmembrane	BF059512
	DTX3L	Deltex 3-like (Drosophila)	AA577672
Apoptosis	*CASP4*	Caspase 4, apoptosis-related cysteine peptidase	U25804
	CASP8	Caspase 8, apoptosis-related cysteine peptidase	NM_001228

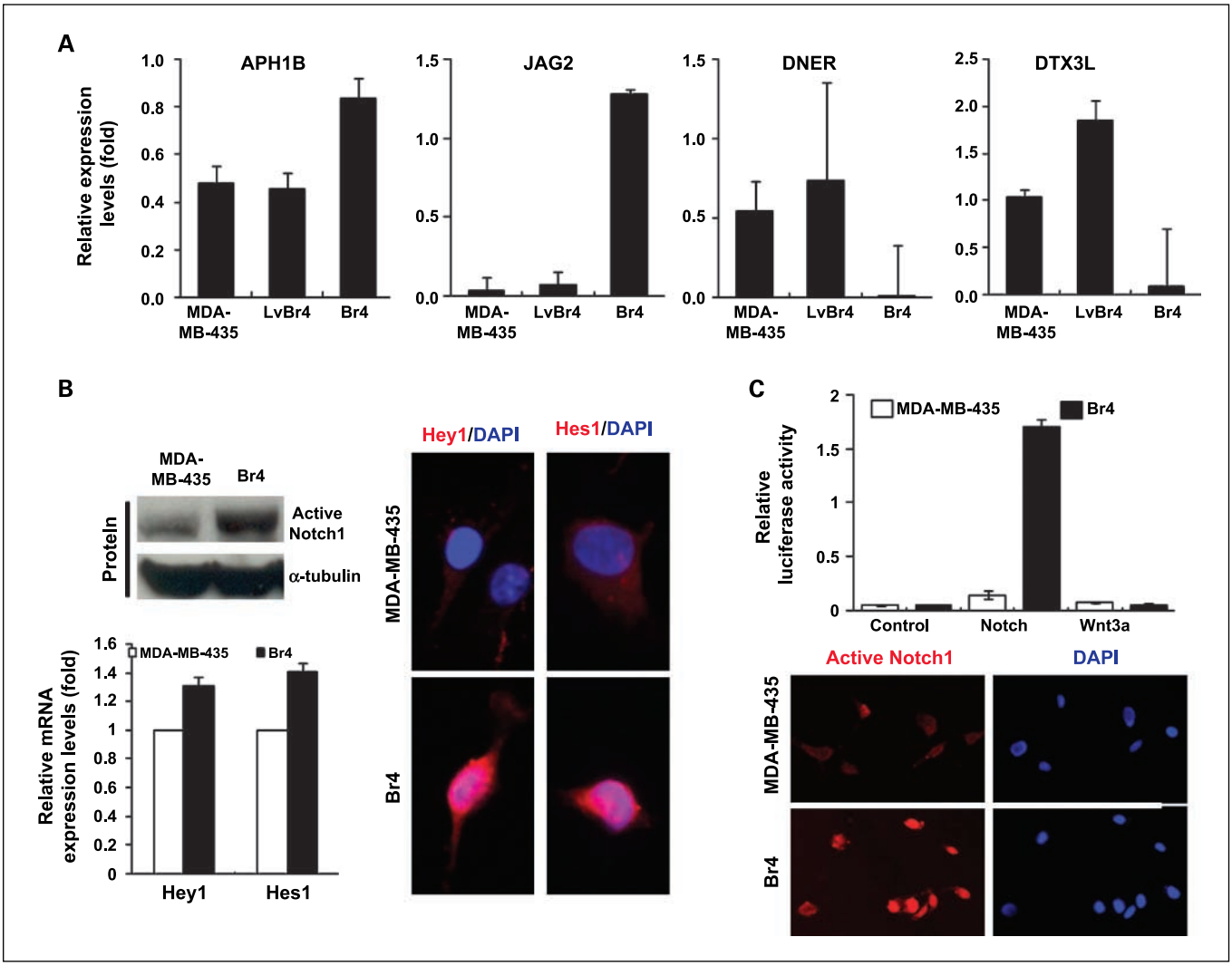

Fig. 3. Activation of Notch signaling in Br4 cells. *A,* expression of genes for Notch signaling in MDA-MB-435 and Br4 cells were determined by real-time RT-PCR ($n = 3$). APH1B, anterior pharynx defective 1b homologue; JAG2, Jagged2; Dner, Δ/Notch-like epidermal growth factor – related receptor; and DTX3L, deltex 3 – like (Drosophila). *B,* increased active form of Notch (NICD) in the MDA-MB-435 and Br4 cells was determined by Western blot analysis ($n = 4$). The α-tubulin was used as a protein loading control (*top left*). Expression levels of Hey1 and Hes1 mRNAs were determined by semiquantitative RT-PCR ($n = 3$; *bottom left*). Expression of Hey1 and Hes1 proteins were analyzed by immunofluorescence analysis (*right*; magnification ×100). *C,* relative Notch transcriptional activity in the MDA-MB-435 and Br4 cells was determined by Notch/CSL luciferase-reporter assay (*top*). Expression of active Notch1 (cleaved Notch1) was analyzed by immunofluorescence analysis (*bottom;* magnification, ×40).

uncoated and collagen-coated transwell culture conditions, respectively (Fig. 5B). Taken together, these results strongly suggest that increased migration of the Br4 cells is attributed to active Notch signaling.

Discussion

Metastases of breast cancers are hardly detectable many years after the surgical removal of primary tumors, whereas small cell lung cancer is usually detected with metastases following the initial diagnosis. The potential of metastasis can be predicted from clinical features such as tumor size, histologic grade, and gene expression patterns (13). In this article, we have developed a brain metastasis model of breast cancer using repeated injections of cancer cells into the ICA. Gene expression profiling data revealed many interesting changes in Br4 cells, and we have shown the role of Notch signaling in brain metastasis by functional analysis on the migration of Br4 cells.

The brain-selected Br4 cells do not make tumors in the mammary fat pad, however, they can metastasize to the lungs. When Br4 cells were injected in the ICA of nonobese diabetic/severe combined immunodeficiency and Nude mice, brain lesions grew in an aggressive manner, and significantly diminished the survival of the mice. These findings suggest that Br4 cells have an affinity for brain and lung metastases and are well-adapted to these microenvironments. Certain factors are associated with the tumor engraftments as well as growth at the brain.

Metastasis is a multistep and multifunctional biological cascade that is the final and most life-threatening stage of cancer progression. From xenograft models of breast cancer metastasis, gene expression studies have suggested organ-specific patterns of metastatic colonization (14). These data show that a subset of site-specific metastasis genes seemed to be selected early in tumor progression. We compared our profiles from the brain metastasis model with previous

metastasis models to test whether the basic mechanism for metastasis might be shared between metastasis models. From the partial list of genes selected from the reported lung metastasis model, we found 6 out of 18 genes in common; *KYNU*, *ID1*, *MAN1A1*, *NEDD9*, *TNC*, and *FSCN1* (15). Although we did not compare the whole expression patterns, the small numbers of overlap support the idea of organ-specific metastasis.

Recent evidence has been documented that the activation of Notch signaling by hypoxia is directly associated with cell fate determination and survival in various cells types (16). Furthermore, overexpression of Notch-1 and its ligands (Delta-like-1 and Jagged-1) was critical for cell survival and proliferation of glioma cells (17). Although we showed that activation of Notch signaling by overexpression of Jagged-2 ligand promotes cell migration and invasion of brain-metastatic Br4 cells, it remains unclear whether the activated Notch signaling is directly involved in a brain-specific metastasis of the Br4 cells. Br4 cells failed to form local tumors in the mammary fat pad, yet they did metastasize to the lungs, hence the activation of Notch signaling in these cells might not be the only critical factor for metastasis to the brain. However, it is possible that Notch signaling might play a crucial role in the survival of Br4 cells in a microenvironment such as the brain, but not in the mammary fat pad.

According to our findings in which inhibition of Notch signaling by DAPT led to a marked decrease of cell migration in Br4 cells, it is also plausible that not only inhibition of Notch signaling, but also other cell-cell adhesion molecules, such as E-cadherin, which is cleaved by presenilin 1 (one of the γ-secretase multicomplex components), might be involved in robust migration and invasion of the Br4 cells (18). Furthermore, a number of preclinical studies have shown that targeting of Notch signaling using γ-secretase

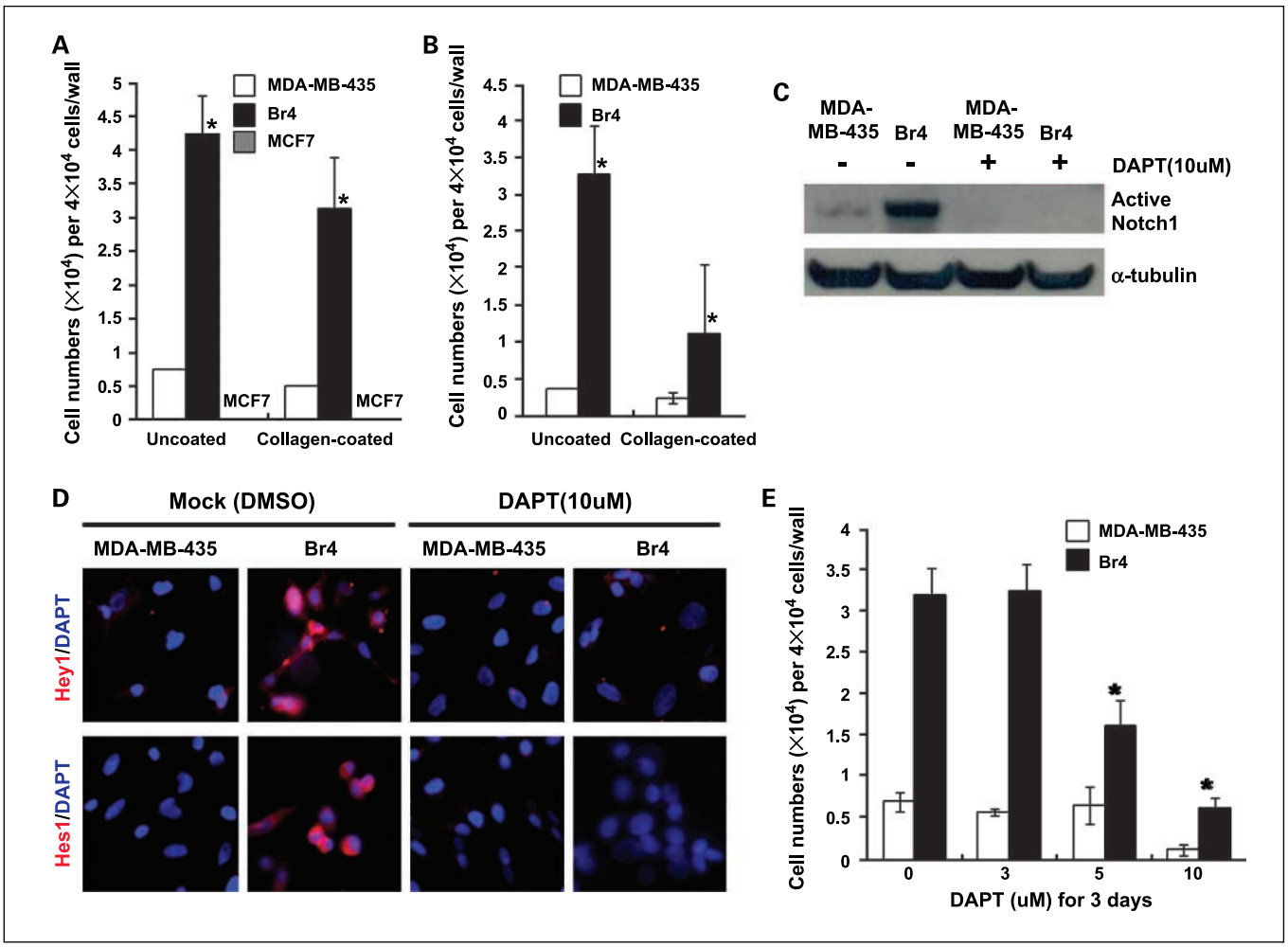

Fig. 4. Increased migration and invasion rates of the Br4 cells are suppressed by inhibition of Notch signaling using DAPT, a γ-secretase inhibitor. *A, in vitro* cell migration of MDA-MB-435, Br4, and MCF7 (as a negative control) was analyzed using a transwell culture system. Cell numbers, the number of cells which migrated from the upper chambers (coated without or with collagen) to the lower chambers for 72 h. *, $P < 0.01$, statistical difference between MDA-MB-435 and Br4 cells ($n = 3$). *B, in vitro* cell invasion of MDA-MB-435 and Br4 cells. Cell numbers, the number of cells which migrated from the upper chambers (coated without or with Matrigel) to the lower chambers for 72 h. *, $P < 0.05$, statistical difference between MDA-MB-435 and Br4 cells ($n = 3$). *C,* expression levels of active Notch1 in MDA-MB-435 and Br4 cells grown in the absence or presence of DAPT (10 μmol/L) for 3 d were determined by Western blot analysis. The α-tubulin was used as a protein loading control (*top left*). *D,* expression levels of Hey1 and Hes1 proteins in MDA-MB-435 and Br4 cells grown in the absence (Mock) or presence of DAPT (10 μmol/L) for 3 d were analyzed by immunofluorescence analysis (magnification, ×40). *E, in vitro* cell migration of the MDA-MB-435 and Br4 cells that were allowed to grow in the different concentrations of DAPT (0, 3, 5, and 10 μmol/L) for 3 d. *, $P < 0.05$, statistical difference among Br4 cells grown in the different concentrations of DAPT ($n = 3$).

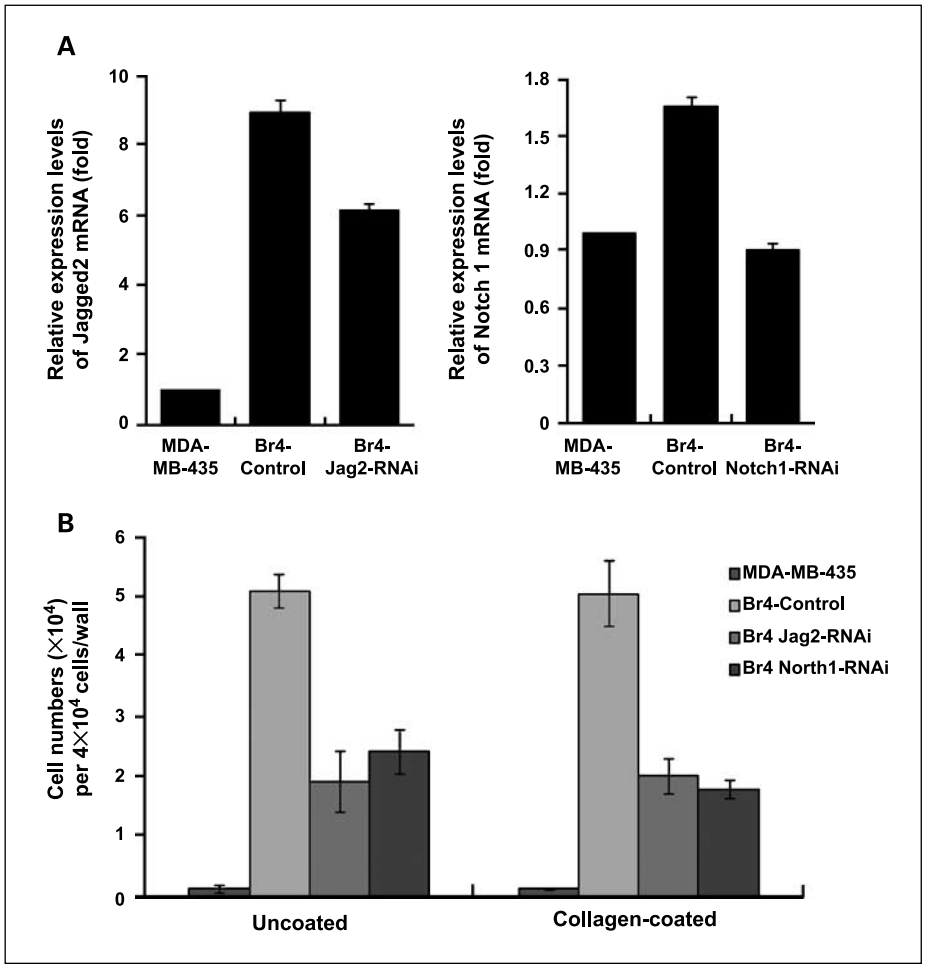

Fig. 5. Increased migration and invasion rates of the Br4 cells are inhibited by the RNAi-mediated depletion of Jagged2 and Notch1 expression. *A,* expression levels of Jagged2 in the MDA-MB-435, Br4-Control, and Br4 cells transduced with Jagged2-specific RNAi vector (Br4-Jag2-RNAi) were determined by semiquantitative RT-PCR. Expression levels of Notch1 in the MDA-MB-435, Br4-Control, and Br4 cells transduced with Notch1-specific RNAi vector (Br4-Notch1-RNAi) were determined by semiquantitative RT-PCR. *B, in vitro* cell migration and invasion of MDA-MB-435, Br4-Control, Br4-Jag2-RNAi-1, and Br4-Notch1-RNAi-1 cells were analyzed using a transwell culture system. Cell numbers, the number of cells which migrated from the upper chambers (coated without or with collagen) to the lower chambers for 72 h (n = 3).

inhibitors, such as DAPT, showed a clinically promising outcome in patients with cancer (19). Therefore, it is suggestive that brain metastasis of the patients with breast cancer might also be suppressed by treatment of γ-secretase inhibitors. However, before considering γ-secretase inhibitors as therapeutics for brain metastasis, more precise roles of Notch signaling in the brain metastasis should be addressed in future studies.

Disclosure of Potential Conflicts of Interest

No potential conflicts of interest were disclosed.

Acknowledgments

We thank Y-J. Choi for her assistance in the Genomics Core Facility of IGMI, and Seoul National University College of Medicine for the experiments and analysis of Affymetrix microarrays.

References

1. Minn AJ, Gupta GP, Siegel PM, et al. Genes that mediate breast cancer metastasis to lung. Nature 2005;436:518–24.
2. Sørlie T, Tibshirani R, Parker J, et al. Repeated observation of breast tumor subtypes in independent gene expression data sets. Proc Natl Acad Sci U S A 2003;100:8418–23.
3. van de Vijver MJ, He YD, van't Veer LJ, et al. A gene-expression signature as a predictor of survival in breast cancer. N Engl J Med 2002;347:1999–2009.
4. Wang Y, Klijn JG, Zhang Y, et al. Gene-expression profiles to predict distant metastasis of lymph-node-negative primary breast cancer. Lancet 2005;365:671–9.
5. Suzuki M, Mose ES, Montel V, Tarin D. Dormant cancer cells retrieved from metastasis-free organs regain tumorigenic and metastatic potency. Am J Pathol 2006;169:673–81.
6. Ward EJ, Shcherbata HR, Reynolds SH, Fischer KA, Hatfield SD, Ruohola-Baker H. Stem cells signal to the niche through the Notch pathway in the Drosophila ovary. Curr Biol 2006;16:2352–8.
7. Miele L, Golde T, Osborne B. Notch signaling in cancer. Curr Mol Med 2006;6:905–18.
8. Iso T, Kedes L, Hamamori Y. HES and HERP families: multiple effectors of the Notch signaling pathway. J Cell Physiol 2003;194:237–55.
9. Price JE, Polyzos A, Zhang RD, Daniels LM. Tumorigenicity and metastasis of human breast carcinoma cell lines in nude mice. Cancer Res 1990;50:717–21.
10. Kim JH, Ha IS, Hwang CI, et al. Gene expression profiling of anti-GBM glomerulonephritis model: the role of NF-κB in immune complex kidney disease. Kidney Int 2004;66:1826–37.
11. Lee MS, Jun DH, Hwang CI, et al. Selection of neural differentiation-specific genes by comparing profiles of random differentiation. Stem Cells 2006;24:1946–55.
12. Kim J, Chung HJ, Park WY, Kim JH. ChromoViz: multimodal visualization of gene expression data onto chromosomes using scalable vector graphics. Bioinformatics 2004;20:1191–2.
13. Minn AJ, Gupta GP, Padua D, et al. Lung metastasis genes couple breast tumor size and metastatic spread. Proc Natl Acad Sci U S A 2007;104:6740–5.
14. Gustafsson MV, Zheng X, Pereira T, et al. Hypoxia requires Notch signaling to maintain the undifferentiated cell state. Dev Cell 2005;9:617–28.
15. Purow BW, Haque RM, Noel MW, et al. Expression of Notch-1 and its ligands, Δ-like-1 and Jagged-1, is critical for glioma cell survival and proliferation. Cancer Res 2005;65:2353–63.
16. Gupta GP, Minn AJ, Kang Y, et al. Identifying site-specific metastasis genes and functions. Cold Spring Harb Symp Quant Biol 2005;70:149–58.
17. Minn AJ, Kang Y, Serganova I, et al. Distinct organ-specific metastatic potential of individual breast cancer cells and primary tumors. J Clin Invest 2005;115:44–55.
18. Marambaud P, Shioi J, Serban G, et al. A presenilin-1/γ-secretase cleavage releases the E-cadherin intracellular domain and regulates disassembly of adherens junctions. EMBO J 2002;21:1948–56.
19. Shih I-M, Wang T-L. Notch signaling, γ-secretase inhibitors, and cancer therapy. Cancer Res 2007;67:1879–82.

Clinical Cancer Research

Activation of Notch Signaling in a Xenograft Model of Brain Metastasis

Do-Hyun Nam, Hye-Min Jeon, Shiyeon Kim, et al.

Clin Cancer Res 2008;14:4059-4066.